Int. J. Electrochem. Sci., 16 **(2021)** Article Number: 211210, doi: 10.20964/2021.12.17

International Journal of
ELECTROCHEMICAL
SCIENCE
www.electrochemsci.org

Synthesis of $NiSe_2$ Nanoparticles Embedded into Carbon Nanoplate as Lithium/Sodium Ion Battery Anodes

Xiuhua Zhang, Taozhi Zhang, Ruijuan Zheng, Chenhao Zhao[*]*, Yunlong Zhou and Zhibiao Hu*

Fujian Provincial Key Laboratory of Clean Energy Materials, College of Chemistry & Materials, Longyan University, Fujian Longyan, China, 364000.
[*]E-mail: 360188044@qq.com

Received: 26 July 2021 / *Accepted:* 23 September 2021 / *Published:* 10 November 2021

Transition metal selenide $NiSe_2$ can be readily obtained via solid state or gas diffusion route between Ni based compounds and elementary selenium. In the present study, the $NiSe_2$/C composite has been prepared from Ni/C composite directed selenium gas diffusion route. The $NiSe_2$ with a cubic phase possesses a size of 100-200 nm, uniformly embedded into carbon nanoplate, which is observed by scanning or transmission electron microscope. As anode materials of lithium or sodium ion batteries (LIBs or SIBs), the comparative electrochemical performances among $NiSe_2$/C composite, bare $NiSe_2$, and carbon have been studied. The results show that the $NiSe_2$/C composite can deliver a discharge capacity of 490.3 mAh/g after 100 cycles at 0.2 A/g as LIBs anode, while the pure carbon can retain a discharge capacity of 441.8 mAh/g at the same condition. Consideration of lower charge voltage of carbon, it may be a better candidate as LIBs anode. However, the presence of $NiSe_2$ can effectively improve the discharge capacity and initial Coulombic efficiency as SIBs anode. The $NiSe_2$/C composite can deliver a reversible discharge capacity of 341.3 mAh/g and moderate cycling stability, while bare $NiSe_2$ has poor cycling stability in either LIBs or SIBs anode.

Keywords: $NiSe_2$ nanoparticles; carbon nanoplate; comparative electrochemical performances; lithium/sodium ion batteries; anode materials.

1. INTRODUCTION

In decades, transition metal chalcogenides have been given extensive research such as lithium ion batteries (LIBs) or sodium ion batteries (SIBs) anodes due to their high discharge capacity [1-3]. Among all metal chalcogenides, metal selenides have been regarded as one of the most promising SIBs anodes [4-7]. Interestingly, it has been proved that the lithium storage performance of metal selenides is also not bad [8-10]. Generally speaking, the theoretical discharge capacity (based on pure faradic contribution) of metal selenides is lower than analogy metal oxides or sulfides. However, the reported discharge capacity of metal selenides can reach 600 mAh/g or above, and the excessive capacity

should come from pseudo-capacity (double-layer diffusion process) contribution [11,12]. Furthermore, the good overlap orbit between 3d of transition metal and 4p of Se, as well as low electronegativity of Se, let the metal selenides possess good electron conductivity [13], which is an important parameter for high-performance electrode materials.

Nickel selenides ($NiSe_x$), one of the common metal selenides including NiSe [14], $Ni_{0.85}Se$ [15, 16], Ni_3Se_4 [17] and $NiSe_2$ [18-20] have been given much attention as SIBs/LIBs anodes or electrochemical catalysts. In comparison with other nickel selenides, $NiSe_2$ with cubic phase exhibits good performances as electrode material. Importantly, $NiSe_2$ can be readily obtained in the presence of enough selenium and a high reaction temperature. Generally, high temperature assisted gas diffusion selenization or solid state reaction between Ni based compound and elementary selenium can be used to prepare $NiSe_2$, and the structure and morphology of $NiSe_2$ is determined by its precursor template (i.e., Ni based compound) [3, 4, 18-20]. For instance, the $NiSe_2$ micros-nano spheres with hierarchical structure can be obtained from $Ni(OH)_2$ spheres template using solid state reaction [21].

Besides the selection preparation of different $NiSe_x$, it also has been widely proved that the combination of $NiSe_2$ with carbon was essential for electrode materials. The existence of carbon can not only buffer the volume change during cycling, but also increase the electron conductivity [3, 4, 18, 20]. However, several studies also report the bare $NiSe_2$ can deliver good electrochemical performances [19, 21]. Furthermore, the lithium or sodium storage ability of carbon in the composite may be not very clear due to less mentioned. In view of above, the $NiSe_2$/carbon composite that $NiSe_2$ nanoparticles encapsulated into carbon nanoplate has been prepared from Ni/carbon composite, which is derived from citric acid-Ni-urea gel. Especially, the comparative lithium/sodium storage performances among this composite, pure carbon and $NiSe_2$ have been studied in the text.

2. EXPERIMENTAL

All of the reagents are analytical grade without further purification, $NiSe_2$/carbon composites were prepared by template directed gas diffusion selenization route as follows:

2.1 Synthesis of Ni/C composite

Ni/C composites were prepared according to Su's route [22]. 5 g urea, 1.0 g citric acid, and 0.4 g $NiCl_2 \cdot 6H_2O$ were dissolved in a mixed solution of 50 mL distilled water and 150 mL ethanol. The green solution was kept at 85 ^oC with magnetic stirring until green gel was formed. The wet gel was dried at 80 ^oC overnight and transferred to a porcelain boat, which was heated at 350 ^oC for 2 h and then 700 ^oC for 4 h in a tube furnace with flowing Ar at a heating rate of 5 ^oC per minute. After cooling to room temperature, the sample was ground into powder for use.

2.2 Synthesis of $NiSe_2$/C composite

A gas diffusion selenization route was carried out to prepare $NiSe_2$/C composite [12]. 0.05 g above Ni/carbon composite and 1 g selenium powder were placed into porcelain boat. Both of them

were transferred to the middle position of a tube furnace, and selenium need to be kept at gas inlet position. Gas diffusion selenization happened at a temperature of 400ºC for 4 h with flowing Ar. The $NiSe_2$/C composite can be obtained after cooling to room temperature. For a comparative purpose, the pure carbon was prepared without addition of $NiCl_2 \cdot 6H_2O$ and $NiSe_2$ was obtained at the presence of 0.6 g $NiCl_2 \cdot 6H_2O$ by same way.

2.3 Structural characterization

The morphologies and size of composites were observed by scanning electron microscope (SEM, Hitachi S-3400) and Transmission electron microscope (TEM, JEOL JEM-2100F). The phase and crystallinity of samples were derived on X-ray diffraction patterns which were collected by X-ray diffractometers (PANalytical X'Pert Powder3) at an accelerating voltage of 40 kV and current of 40 mA. X-ray photoelectron spectrums (XPS, Escalab 250Xi, Thermo) were carried out to confirm the chemical valence and state of Ni/C and $NiSe_2$/C composite. The carbon content of $NiSe_2$/C was calculated based on Thermogravimetric analysis (TGA□DSC200PC, Netzsch), which was proceeded from room temperature to 800 ºC at a heating rate of 5 ºC/min under air.

2.4 Electrochemical performances

Working electrode with the active component of $NiSe_2$/carbon composite was prepared as follows: active $NiSe_2$/carbon composite, binder sodium binder, and acetylene carbon are well mixed with ratio of 7:1:2 in an agate mortar. Then, the mixture was transported to a porcelain crucible, and a certain amount of distilled water was added until a slurry was obtained. Sequently, the slurry was uniformly painted on a copper foil, and then dried at 80ºC for ~5h, and the decorated foil was cut into a disk with a diameter of 14 mm. The loading density of the active component on each disc was about 1 mg/cm^2.

A two-electrode style was used to evaluate the electrochemical performances as LIBs anodes, in which, above painted copper disc was used as working electrode, and lithium plates with diameter of ~14.5 mm used as reference/counter electrode. Commercial LBC-301 purchased from Shenzhen CapChem or Celgard 2400 was used as electrolyte or separator, respectively. CR2016 coin cell was assembled in a high-purity Ar filled glove box. When evaluated as SIBs anode, except a homemade sodium plate with a diameter of 15 mm or $NaCF_3SO_3$ DEGDME solution (1 mol/L, Mojiesi) was used as reference/counter electrode or electrolyte, respectively, the other procedure was same with former (lithium ion coin cell) assembly.

Constant current charge-discharge tests were performed in a CT-3008 battery test system (Shenzhen Neware) with a voltage window of 0.01-2.8 V at different current densities. Cyclic voltammetry (CV) profiles were obtained from an electrochemical workstation (CHI660C Shanghai Chenhua) within 0.01-2.8 V at different scanning rates.

3. RESULTS AND DISCUSSION

3.1 Structural characterization

In order to obtain $NiSe_2$/C composites with confined size and good distribution, a Ni/carbon composite directed selenization route is applied. The schematic formation process of $NiSe_2$/carbon composite is revealed in Fig. S1, and the Ni-citric acid-urea gel results in the formation of a Ni/C composite that Ni nanoparticles encapsulated into carbon nanoplate. Then, in the presence of selenium vapor (during gas phase diffusion), a combination reaction between elementary Ni and Se instead of ion-exchange reaction is easy to happen due to the immediate formation of a new chemical bond.

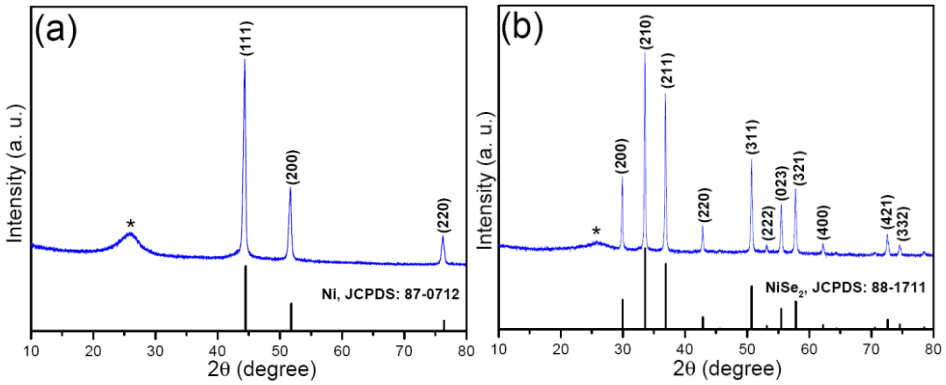

Figure 1 XRD patterns of (a) Ni/C composite and (b) $NiSe_2$/C composite, the wide peak marked by asterisk suggests the presence of carbon

Fig.1 shows XRD pattern of Ni/C composite and corresponding $NiSe_2$/C composite. The pattern of precursor Ni/carbon composite can well match with the standard profile of metallic Ni (JCPDS: 87-0712) without any impurities. A wide diffraction denoted by an asterisk indicates co-existence of amorphous carbon. These results suggest that the Ni-citric acid-urea gel has been completely transformed into metallic Ni and carbon after synchronous reduction and carbonization. A gas diffusion selenization route is employed to prepare $NiSe_2$/carbon composite, and a combination reaction instead of anion exchange reaction happens during selenization. Fig. 2b reveals XRD pattern of $NiSe_2$/carbon composite, which can be indexed to standard cubic $NiSe_2$ (JCPDS: 88-0711), indicating a successful transformation from metallic Ni to $NiSe_2$ in the presence of Se steam and under certain temperature (400ºC). Also, a wide peak nearby 25º suggests the existence of carbon. In comparison, the pure carbon obtained without the addition of $NiCl_2 \cdot 6H_2O$ possesses an amorphous structure, while the sample obtained at a high ratio of $NiCl_2$ shows a cubic $NiSe_2$ structure (Fig. S2).

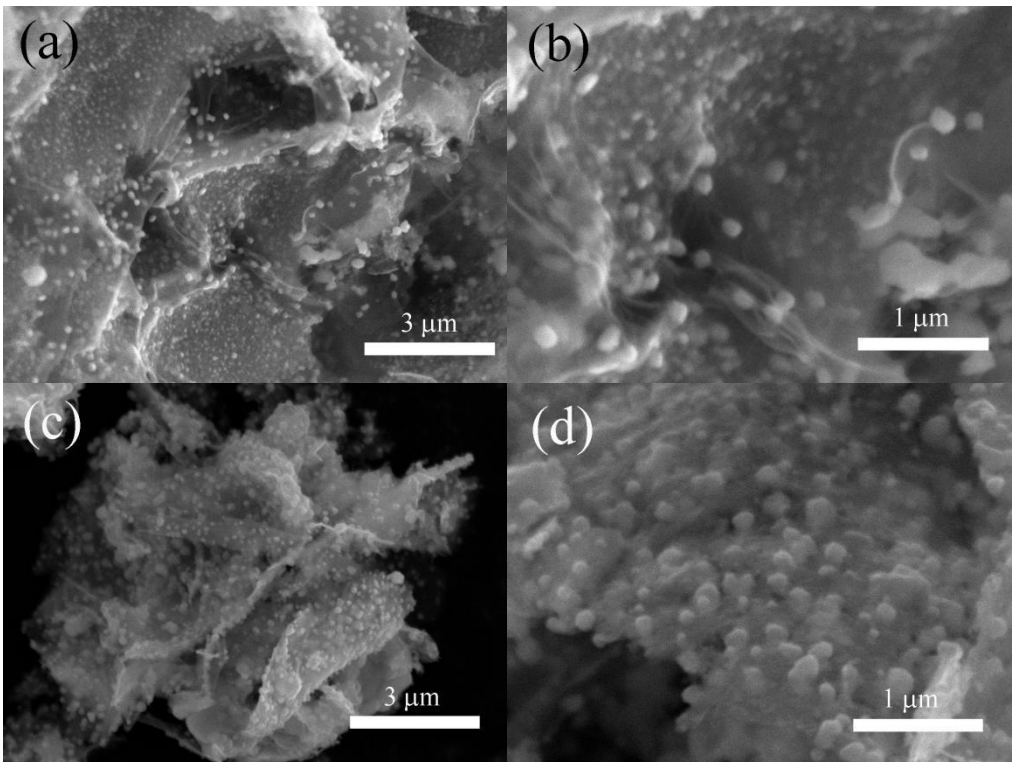

Figure 2 SEM images of (a, b) Ni/C composite and (c, d) $NiSe_2$/C composite

Morphologies, size, and surface structure of Ni/C composite and $NiSe_2$/C composite are observed and shown in Fig. 2. It can be clearly seen that numerous Ni nanoparticles are uniformly encapsulated into the carbon matrix (Fig. 2a), which possesses a thin plate-like structure. In a magnification view, the size of Ni nanoparticles is much smaller than 1 micrometer. This Ni/C composite is derived from Ni-citric acid-urea gel, and the formed carbon from citric acid can inhibit the crystal growth and aggregation of Ni nanoparticles, as well as provide effective carbon interaction. The urea can help to form pore structure during decomposition.

The $NiSe_2$/C composition can be readily obtained through a combination reaction between metallic Ni and Se steam. Fig. 3c shows the SEM images of $NiSe_2$/C composite at an overall view, and the composite inherits the structure of the template that the $NiSe_2$ nanoparticles encapsulated into carbon nanoplates. However, the size of carbon nanoplate turns to be smaller after selenization process [23]. At a close view (Fig. 3d), numerous $NiSe_2$ nanoparticles can be clearly presented, and the size of $NiSe_2$ should be larger nanoparticles due to transformation from elementary Ni to $NiSe_2$. SEM images of pure carbon and $NiSe_2$ are revealed in Fig. S3, the carbon possesses the typical nanosheet structure. As for $NiSe_2$, numerous nanoparticles with hundreds of nanometers in size aggregate due to high-temperature selnization.

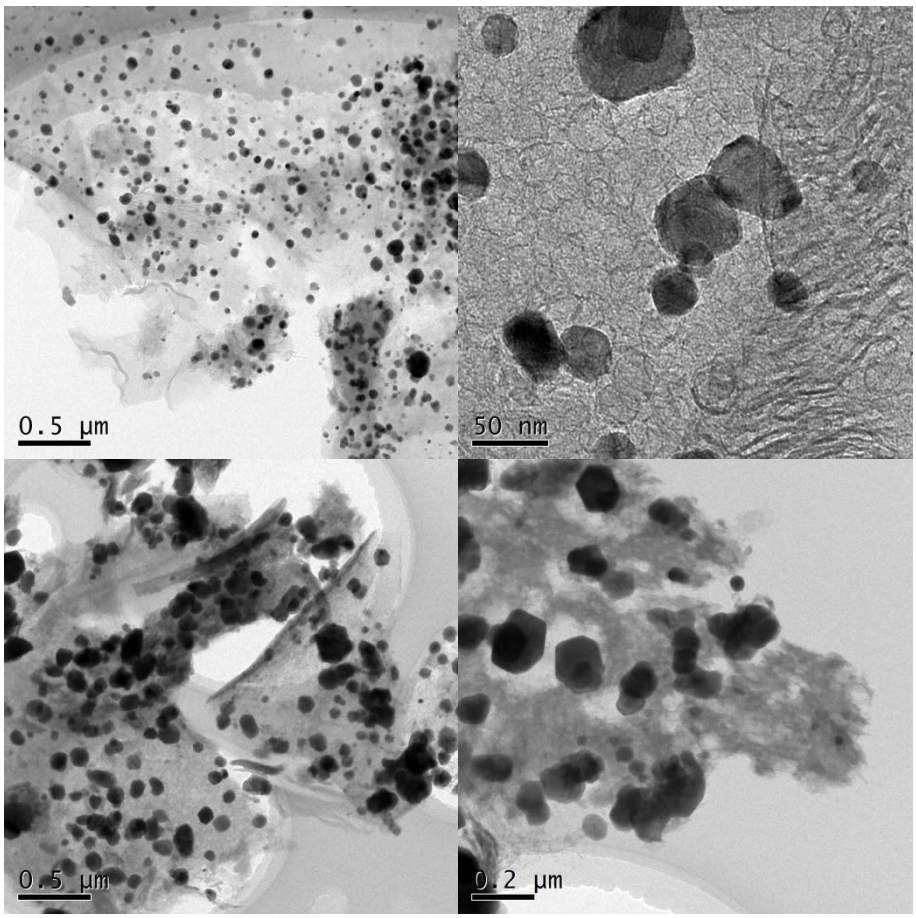

Figure 3 TEM images of (a, b) Ni/C composite and (c, d) $NiSe_2$/C composite

TEM was performed to further present the structure of Ni/C and $NiSe_2$/C composite and the results were shown in Fig. 3. Ni nanoparticles encapsulated into large-area carbon nanoplate can be clearly observed (Fig. 3a), and their size is about 50 nm (Fig. 3b). Also, the TEM of $NiSe_2$/C composite, which is randomly captured, shows similar $NiSe_2$ nanoparticles encapsulated into carbon nanoplate (Fig. 3c). Apparently, it can be seen form Fig. 3b and d, the particle size significantly increases due to selenization of elementary Ni as expected. Furthermore, the particle with clear corner and edge suggests good crystallization.

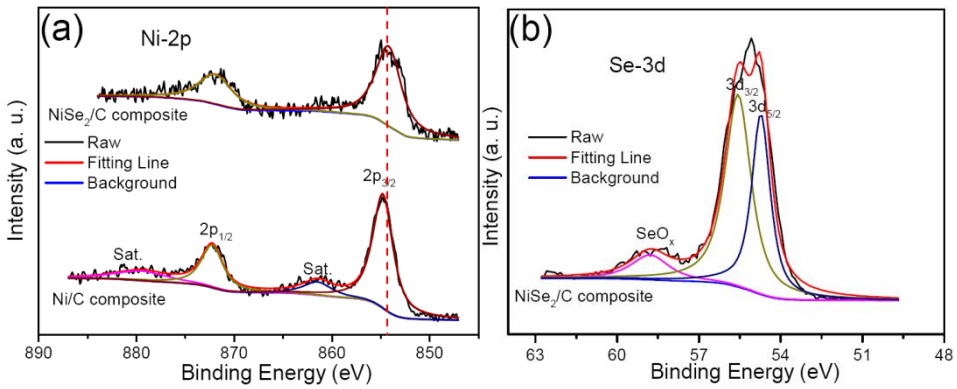

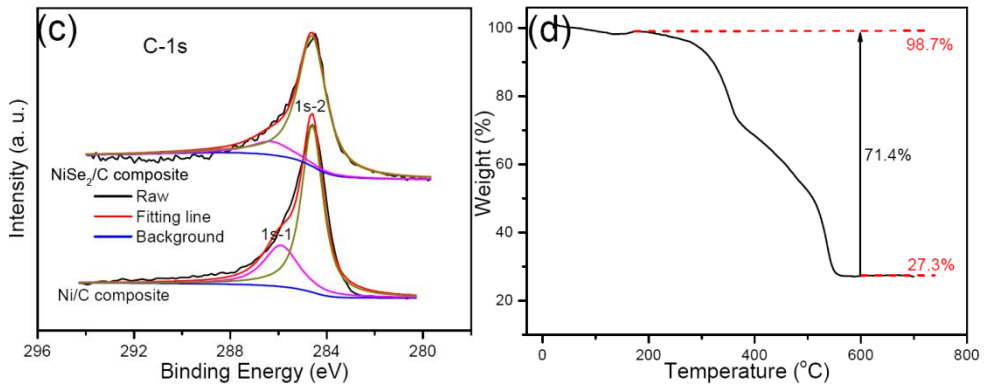

Figure 4 XPS spectra of (a) Ni-2p, (b) Se-3d and (c) C-1S, (d) TG analysis of $NiSe_2$/C composite from room temperature to 800ºC under air

As we know, Ni has a stable chemical valence of +2 even in combination with strong electronegative oxygen (i.e., NiO) due to its half-filled electron structure ($t_{2g}^6e_g^2$) in an octahedral field. Within $NiSe_2$, Ni should keep the same chemical valence [24], The Ni $2p_{1/2}$ or $2p_{3/2}$ binding energy of Ni/C composite locates 872.6 or 855.1 eV [18-20, 24], respectively (Fig. 4a), and both of them are bigger than elementary Ni from NIST database. Consideration of abundant oxygen in the carbon matrix, an interaction between Ni and oxygen may result in its increase. The Ni $2p_{1/2}$ or $2p_{3/2}$ of $NiSe_2$/C composite shift to low energy position with a decrease on peak intensity, and a relatively weaker electrostatic repulsion between Ni and Se compared with oxygen may respond to the change. In general, Se with a chemical valance of -1 possesses a structure of Se_2^{2-} for $NiSe_2$/C composite, and its 3d orbit binding energy is revealed in Fig. 4b. The binding energy at 55.7 or 54.6 eV of can be indexed to the $3d_{3/2}$ or $3d_{5/2}$ orbital, respectively, and a weak peak nearby 58.9 eV corresponds to the formation of SeO_x [18, 19, 25].

The XPS spectrum of C-1s is shown in Fig. 4c. the binding energy of 284.5 eV (1s-2) is the formation of C-C bond, and a weak peak in higher binding energy (1s-1) should be the C-O bond for Ni/C composite, suggesting incomplete carbonization of citric acid. TG analysis of $NiSe_2$/C composite from room temperature to 800 ºC under air is revealed in Fig. 4c. The weight loss from room temperature to 200 ºC should be ascribed to remove of adsorbed water, and a weight loss of 71.4% happens from 200 to 600 ºC accompanying with the combustion of carbon and transformation of $NiSe_2$/C to NiO, and a weight ratio of $NiSe_2$ component can be calculated as ~80.2% according to the above analysis.

3.2 Electrochemical performances

Electrochemical performances of $NiSe_2$/C composite, bare $NiSe_2$, and carbon as LIBs anodes are evaluated in Fig. 5. $NiSe_2$/C composite, bare $NiSe_2$ or pure carbon gives an initial discharge capacity of 943.9, 790.2 or 1243.2 mAh/g, and recover to 583.3, 496.0 or 691.5 mAh/g at 0.2 A/g respectively, delivering an initial Coulombic efficiency of 61.8%, 62.8% or 55.6%, respectively (Fig. 5a). It can be clearly seen that either reversible capacity or Coulombic efficiency of $NiSe_2$/C composite

is in middle. A charge plateau ~ 1.9 V can be found for $NiSe_2$/C composite surrounded by a dotted line, and this phenomenon turns to more obvious for $NiSe_2$, which should be attributed to reduction reaction of Ni based material (Faradic energy storage). Furthermore, the charge voltage of such three materials also can be presented in Fig. 5a, and the pure carbon has a lower voltage, which is a benefit to the whole lithium ion battery.

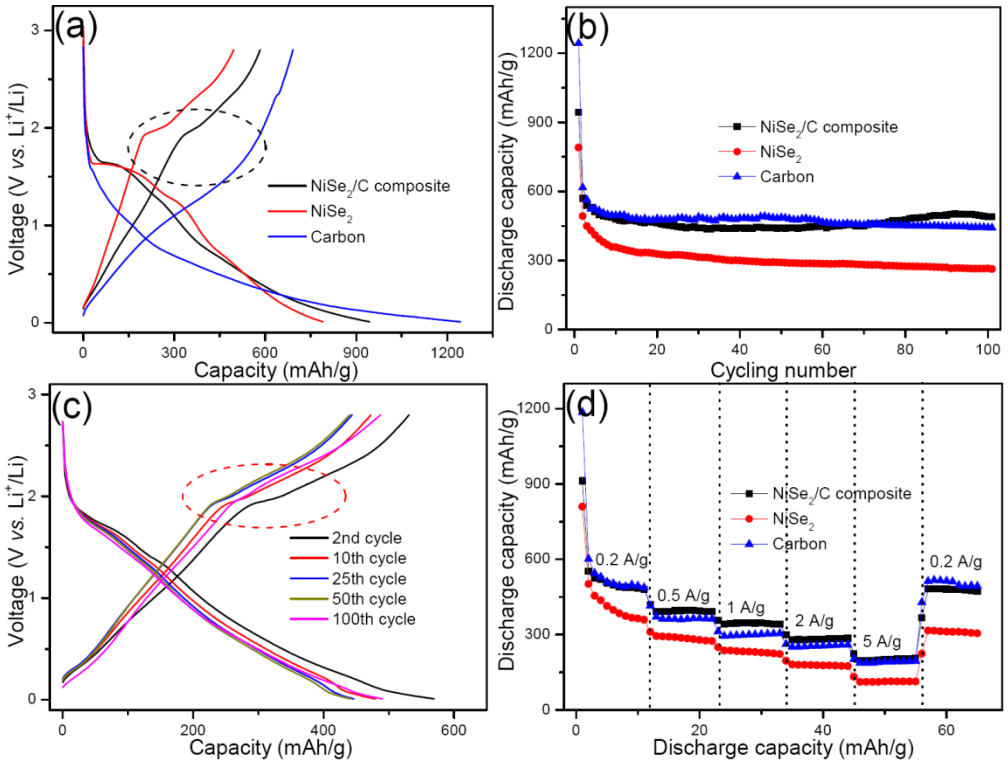

Figure 5 (a) Initial charge-discharge curves and (b) cycling stability at 0.2 A/g of different samples, (c) typical charge discharge curves of $NiSe_2$/C composite and (d) rate capability of different samples as LIBs anodes

Cycling stability of $NiSe_2$/C composite, bare $NiSe_2$, and carbon at 0.2 A/g are revealed in Fig. 5b. The 2nd cycle reversible discharge capacity is 569.4, 492.1 or 616.3 mAh/g for $NiSe_2$/C composite, $NiSe_2$ or carbon, respectively. Then, each sample experiences serious capacity decay for the beginning 10 cycles. After 100 cycles, $NiSe_2$/C composite, $NiSe_2$ or carbon can keep a discharge capacity of 490.3, 262.6 or 441.8 mAh/g. In comparison, the capacity retention ratio of $NiSe_2$/C composite is 86.1%, and it is better than any other sample. As LIBs anode, transition metal chalcogenides encounter volume change during lithiation and delithiation, resulting in bad cycle stability. The presence of carbon nanoplate within $NiSe_2$ nanoparticles can alleviate this influence compared with $NiSe_2$. Typical charge-discharge curves of $NiSe_2$/C composite are revealed in Fig. 5c, a capacity increase happens from 50th to 100th cycles, and there is some difference in charge-discharge profile, that the platform capacity becomes less, especially in charge process (pink line surrounded by dashed), indicating a capacity transformation from faraday to pseudo capacity contribution [26, 27].

Rate capability of various samples is revealed in Fig. 5d. A discharge capacity of 346.0, 228.9 or 301 mAh/g can be obtained for $NiSe_2$/C composite, bare $NiSe_2$ or carbon at 2 A/g and this value decreases to 281.9, 177.7 or 255.7 mAh/g at 5 A/g with a capacity retention of 82.9%, 77.6% or 84.9%. When the current density goes back to 0.2 A/g, the discharge capacity recovers to 482.7, 316.4 or 512.4 mAh/g. Obviously, $NiSe_2$/C composite or carbon nanoplate possesses superior rate capability.

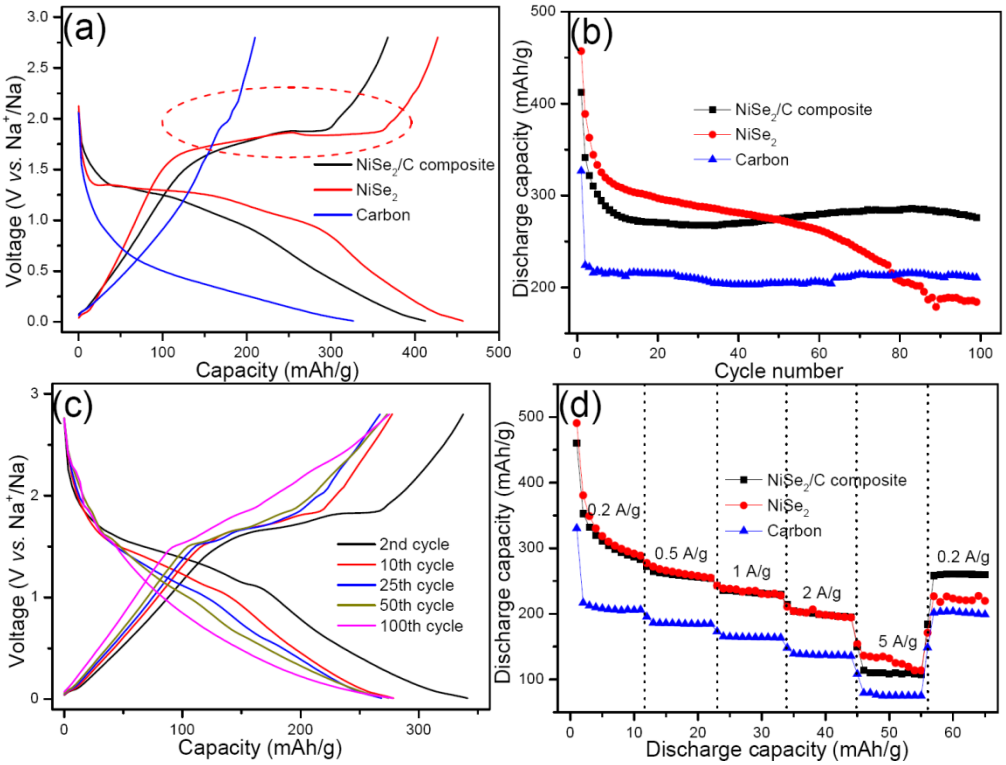

Figure 6 (a) Initial charge-discharge curves and (b) cycling stability at 0.2 A/g of different samples, (c) typical charge discharge curves of $NiSe_2$/C composite and (d) rate capability of different samples as SIBs anodes

Transition metal selenides also have been regarded as good SIBs anodes [18-20], and the electrochemical performances of $NiSe_2$/C composite, bare $NiSe_2$, and carbon are evaluated as shown in Fig. 6. In the initial discharge charge process (Fig. 6a), $NiSe_2$/C composite, bare $NiSe_2$ or carbon delivers a discharge capacity of 412.3, 547.2 or 326.7 mAh/g, and reversible charge capacity of 367.8, 427.1 or 209.8 mAh/g can be recovered, giving an initial Coulombic efficiency of 89.2%, 78.1% or 64.2%, respectively. In comparison, $NiSe_2$ has a much higher sodium storage capacity than carbon, which is different from their performance as LIBs anode. Furthermore, the initial Coulombic efficiency of $NiSe_2$ based materials is high when used as SIBs anode, especially compared with the same data as LIBs anodes, and the charge plateau ~1.8 V becomes more obvious.

The cycling stability of various samples is revealed in Fig. 6b. $NiSe_2$/C composite, bare $NiSe_2$ or carbon delivers a 2^{nd} cycle discharge capacity of 341.3, 388.5, 224.2 mAh/g at 0.2 A/g. After 100 cycles, a capacity value of 276.0, 183.9 or 210.5 mAh/g can be retained. Obviously, the bare carbon

has the best cycling stability, and the $NiSe_2$/C composite can gain a higher capacity value during cycling. However, the cycling stability of electrode materials used as SIBs anode is worse than that used as LIBs anodes. In typical charge-discharge curves (Fig. 6c), it can be found the charge plateau turns unclear, indicating capacity transformation from faraday to pseudo capacity seriously.

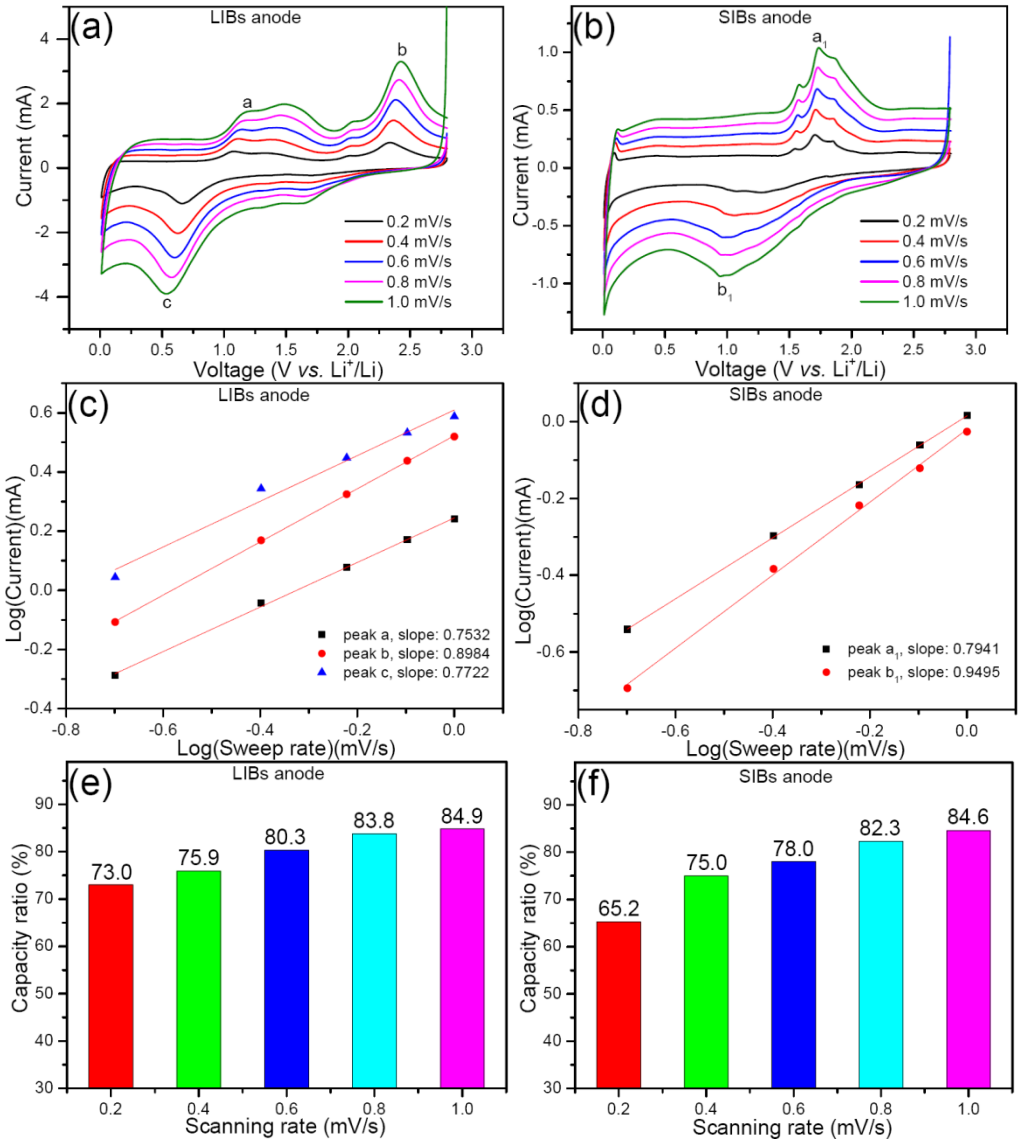

Figure 7. CV curves, linear relation between Log (Current) *vs.* Log (Sweep rate) and capacitive-controlled capacity ratio of $NiSe_2$/C composite at scanning rate from 0.2 to 1.0 mV/s as (a, c and e) LIBs and (b, d and f) SIBs anodes.

Rate capability as SIBs anodes is shown in Fig. 6d. At a high rate of 5 A/g, the composite, bare $NiSe_2$ or carbon delivers a discharge capacity of 110.1, 118.5 or 79.1 mAh/g, respectively, and a capacity of 260.8, 222.3 or 203.4 mAh/g can be recovered at 0.2 A/g for each sample. In comparison, the bare $NiSe_2$ possesses the best rate capability, which is opposite to their performance as LIBs

anodes. In others words, each sample has the worse rate capability as SIBs anodes than that as LIBs anodes, resulting from higher ionic radii of Na^+ and resultant electrochemical reaction kinetics.

It has been proved that the discharge capacity of transition metal selenides has a higher capacity than the theoretical value, and it is composed of the contribution of faraday and pseudo, which can be calculated from CV curves. Fig. 7a reveals the CV curves of $NiSe_2$/C composite as LIBs anode at different current densities, and the anodic peaks marked by *a*, *b*, and cathodic peak marked by *c* can be clearly presented, which should be corresponded to the reversible transformation between $NiSe_x$ and metallic Ni. Interestingly, the CV peaks (Fig. 7b) of $NiSe_2$/C composite as SIBs anode is different from its performance as LIBs, resulting from the influence of carbon and pseudo contribution.

Table 1. Comparison of cycle performanc of NiSe/C with similar anode materials for lithium/sodium ion battery

Materials	Morphology	Battery type	Current rate	Capacity number	Reversible discharge capacity
NiSe/C[14]	Core-shell nanospheres	LIBs	0.2 A g^{-1}	50	428 mAh g^{-1}
		SIBs	0.2 A g^{-1}	50	280 mAh g^{-1}
NiSe/rGO[23]	Hollow microspheres and nanosheets	LIBs	0.4	250	378 mAh g^{-1}
		SIBs	0.05	50	491 mAh g^{-1}
$NiSe_{0.85}$/C[28]	Flowerlike	LIBs	0.2 A g^{-1}	100	480.2 mAh g^{-1}
		SIBs			193.6 mAh g^{-1}
$NiSe_{0.85}$/C[15]	Hollow nanowires	SIBs	0.2 C	100	390 mAh g^{-1}
$NiSe_2$/NC[18]	2D nanocomposites	SIBs	1 A g^{-1}	150	308 mAh g^{-1}
Ni/N-containing C[29]	Nanosheets	LIBs	0.2 A g^{-1}	100	635 mAh g^{-1}
$NiSe_2$/C (This work)	Nanoparticles	LIBs	0.2 A g^{-1}	100	490.3 mAh g^{-1}
		SIBs	0.2 A g^{-1}	100	276 mAh g^{-1}

Furthermore, the peak intensity increase accompanying by the increase of scanning rate, and increase degree is determined by reaction kinetics towards lithium or sodium ion storage. The electrochemical reaction occurring can be classified into a faradaic charge transfer process from faradic (cation intercalation) and pseudo contribution from a double-layer effect, which can be judged from equation [18-20]:

$i_p = av^b$, its derives $\text{Log } i_p = b\text{Log}v + \text{Log}a$

In which, i_p is the peak current, and *v* is the scanning rate. Especially, slope *b* can be used to measure the contribution of capacitive (faradic) or diffusion (pseudo) controlled processes. In detail, when the value of b comes to 1, indicating a complete capacity-controlled behavior, and b reaches 0.5, suggesting a diffusion-controlled process. Fig. 7c or d is the linear relation between Log (Current) *vs.* Log (Sweep rate) as LIBs or SIBs anode. Each peak a, b, c, a_1 or b_1 is higher than 0.75, closing to 1.0, indicating the capacity is inclined to diffusion-controlled process. The accurate diffusion-controlled

fraction in total capacity is revealed in Fig. S4 and Fig. 7. The diffusion capacity contribution to lithium or sodium storage at a scanning rate of 0.2 mV/s is 73.0% and 65.2% (Fig. S4), and this value gradually rises with increased scanning rates. At a high rate of 1.0 mV/s, this contribution reaches 84.9% and 84.6% (Fig. 7e and f), respectively, consistent with the slope analysis in Fig. 7c and d. Importantly, it can be used to explain why the actual discharge capacity of transition metal selenides is higher than theoretical data, and it should be the reason why the metal selenides have good rate capability due to the diffusion-controlled electrochemical process is fast [4, 18-20]. The cycling performance of NiSe/C with similar anode materials for lithium/sodium ion batteries has been summarized in Table 1[14-15,18,23,28-29].In comparison, the $NiSe_2$/C electrode demonstrates substantively cycling stability.

4. CONCLUSION

A template directed gas diffusion selenization route has been developed to prepare the composite that $NiSe_2$ nanoparticles encapsulated into carbon nanoplate. A comparative lithium/sodium storage performance among this composite, bare $NiSe_2$, and carbon has been carried out. The results show that the $NiSe_2$/C composite can deliver a discharge capacity of 490.3 mAh/g after 100 cycles at 0.2 A/g as LIBs anode, while the pure carbon can retain a discharge capacity of 441.8 mAh/g at the same condition. In comparison, pure carbon may be better due to its lower charge voltage. However, the introduction of $NiSe_2$ can effectively elevate the discharge capacity and initial Coulombic efficiency as SIBs anode, and a reversible charge capacity of 367.8 mAh/g, much higher than carbon. In comparison, the cycle stability of bare $NiSe_2$ is poor either as LIBs or SIBs anodes. Furthermore, the analysis on CV curves of $NiSe_2$/C composite indicates the primary capacity contribution is attributed to diffusion-controlled process, and it also can explain why such composite has good rate capability.

ACKNOWLEDGEMENTS
The authors thank the financial supports from Innovative Training Program for College Students (202011312025), and from the Natural Science Foundation of Fujian Province (2021J011092, 2019J01799 and 2019J01800).

SUPPORTING INFORMATION

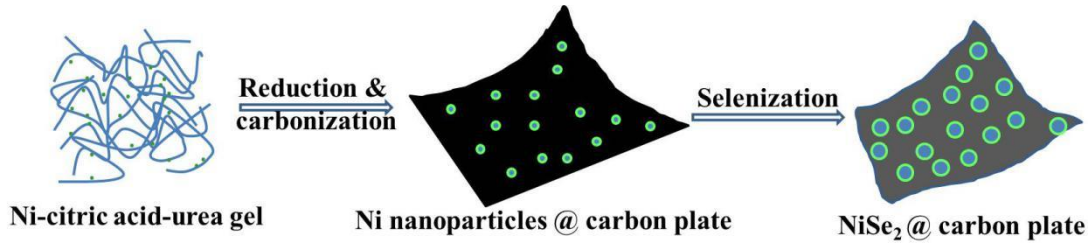

Figure S1 Schematic formation process of $NiSe_2$/C composite

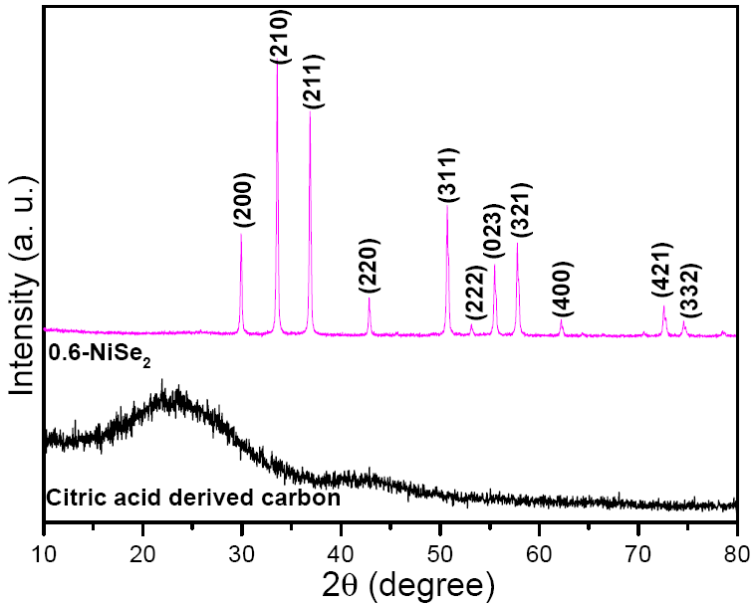

Figure S2 XRD patterns of control sample pure $NiSe_2$ and carbon

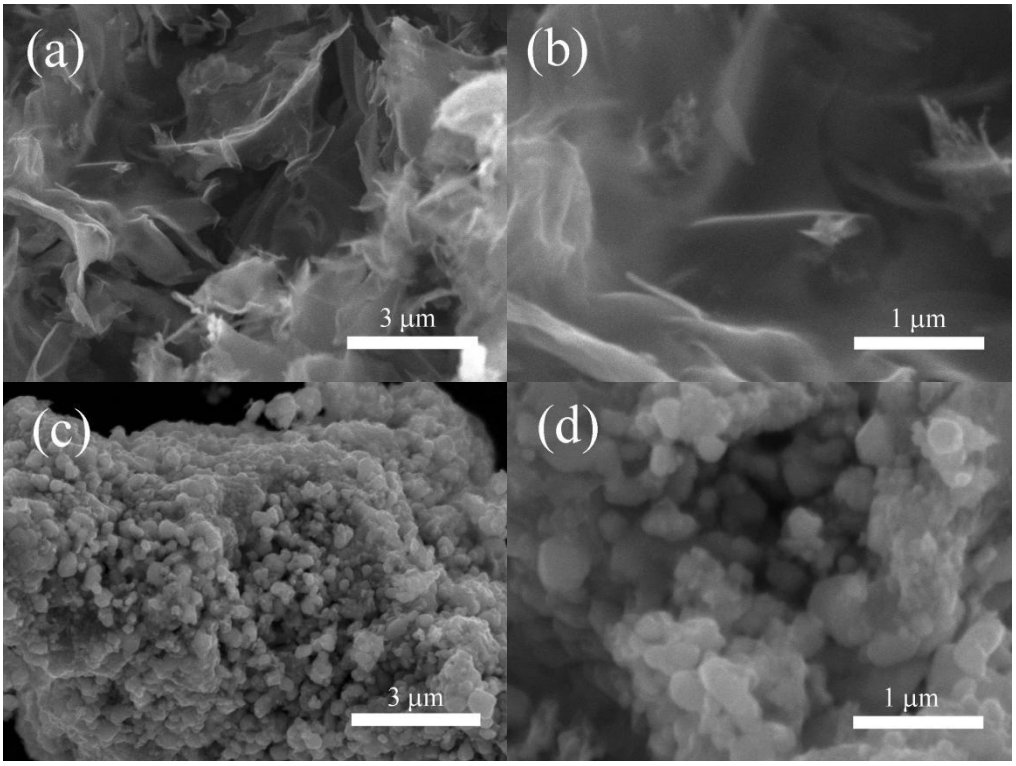

Figure S3 SEM images of control sample (a, b) carbon and (c, d) $NiSe_2$

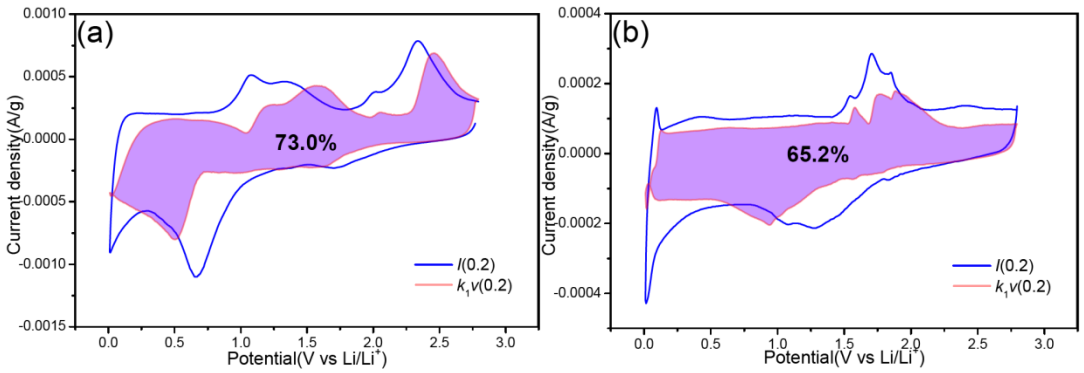

Figure S4 Capacity contribution (purple section) to (a) lithium or (b) sodium storage at scanning rate of 0.2 mV/s

References

1. S. R. Dai, L. C. Wang, M. L. Cao, Z. C. Zhong, Y. Shen, and M. K. Wang, *Mater. Today Energy*, 12 (2019) 114.

2. A. Indra, T. Song, and U. Paik, *Adv. Mater*., 30. 39 (2018) 1705146.
3. M. H. Luo, H. X. Yu, F. Y. Hu, Y. Bai, and J. Shu, *Chem. Eng. J*., 380 (2020) 122557.
4. X. J. Xu, J. Liu, J. W. Liu, R. Z. Hu, and M. Zhu, *Mater.*, 28 (2018) 1707573.
5. D. M. Zhang, J. H. Jia, C. C. Yang, and Q. Jiang, *Energy Storage Mater*., 24 (2020), 439-449.
6. C. X. Lv, H. L. Liu, D. H. Li, S. Chen, H. W. Zhang, X. L. She, and X. X. Gu, *Carbon*, 143 (2019) 106-115.
7. T. Z. Liu, Y. P. Li, L. Z. Zhao, F. H. Zheng, and C. H. Yang, *ACS Appl. Mater. Interface*, 11 (2019) 19040-19047.
8. Q. N. Ma, Q. Y. Zhuang, H. Song, C. M. Mao, and G. C. Li, *Mater. Lett*., 228 (2018) 235-238.
9. J. Yang, H. C. Gao, S. Men, X. W. Kang, and S. W. Chen, *Adv, Sci*., 5 (2018) 1800763.
10. S. H. Zhu, C. Chen, P. He, S. S. Tan, F. Y. Xiong, Z. Liu, Q. Y. An, and L. Q. Mai, *Nano Res*., 12 (2019) 1371-1374.
11. P. Ge, C. Y. Zhang, H. S. Hou, L. Q. Mai, and X. B. Ji, *Nano Energy*, 48 (2018) 617-629.
12. Z. Ali, M. Asif, X. X. Huang, T. Y. Tang, Y. L. Hou, *Adv. Mater*., 30 (2018) 1802745.
13. F. M. Wang, Y. C. Li, T. A. Shifa, K. L. Liu, F. Wang, Z. X. Wang, P. Xu, Q. S. Wang, and J. He, *Angew. Chem. Int. Ed*., 55 (2016) 6919-6924.
14. Z. A. Zhang, X. D. Shi, and X. Yang, *Electrochim. Acta*, 208 (2016) 238-243.
15. X. M. Yang, J. L. Zhang, Z. G. Wang, H. K. Wang, C. Y. Zhi, D. Wu, and A. Rogach. *Small*, 14 (2017) 1702669.
16. X. R. Zheng, X. P. Han, H. Liu, J. J. Chen, D. J. Fu, J. H. Wang, C. Zhong, Y. D. Deng, and W. B. Hu, *ACS Appl. Mater. Interfaces*, 10 (2018) 13675-13684.
17. L. Lv, Y. C. Chang, X. Ao, Z. S. Li, G. Hong, and C. D. Wang. *Mater. Today Energy*, 17 (2020) 100462.
18. S. T. Liu, D. Li, G. J. Zhang, D. D. Sun, J. S. Zhou, and H. H. Song, *ACS Appl. Mater. Interfaces*, 40 (2018) 34193-34201.
19. S. H. Zhu, Q. D. Li, Q. L. Wei, R. M. Sun, X. Q. Liu, Q. Y. An, and L. Q. Mai, *ACS Appl. Mater. Interfaces*, 9 (2017) 311-316.
20. H. Mei, L. Zhang, K. L. Zhang, J. H. Gao, B. Xu, and D. F. *Sun, Acta*, 357 (2020) 136866.
21. Y. Y. He, M. Luo, C. F. Dong, X. Y. Ding, Y. T. Qian, and L. Q. Xu, *J. Mater. Chem.* A, 7 (2019) 3933-3940.
22. L. W. Su, Z. Zhou, and P. W. Shen, *J. Phys. Chem*. C, 45 (2012) 23974-23980.

23. C. H. Zhao, Z. Shen, F. Z. Tu, and Z. B. Hu, *J. Mater. Sci.,* 55 (2020) 3495-3506.
24. M. J. Yi, C. Q. Zhang, C. Cao, C. Xu, B. S. Sa, D. P. Cao, and H. B. Zhan, *Inorg. Chem*., 58 (2019) 3916-3924.
25. X. D. Li, W. D. Zhang, Y. Feng, W. Li, P. Peng, M. C. Li, and C. H. Jiang, *Electrochim. Acta*, 294 (2019) 173-182.
26. S. Q. Zhao, Z. W. Wang, Y. Li, S. Wang, Q. Shen, and Z. Q. Lin. *Adv Energy Mater*, 9 (2019) 1901093.
27. S. Q. Zhao, F. Feng, F. Q. Yu, and Q. Shen, *J. Mater. Chem*. A, 3. 47 (2015) 24095-24102.
28. Y. Liu, and X. Wang, *Materials*, 12. 22 (2019) 3709.
29. L. Su, Z. Zhou , and P. Shen , *J. Phys. Chem*. C, 116.45 (2015) 23974-23980.